JET–CP(98)04

The Role of Recycling and Impurity Production in JET Hot-ion H-modes

H Y Guo, B Balet, G Conway, G Corrigan, S Davies, B de Esch, M von Hellermann, L D Horton, H Lingertat, P Lomas, G F Matthews, G M McCracken, R D Monk, M F F Nave[1], V Parail, R Simonini, R Smith, M Stamp, P C Stangeby[2], A Tabasso, A Taroni, P Thomas, K-D Zastrow.

JET Joint Undertaking, Abingdon, Oxfordshire, OX14 3EA,
[1]Associaçáo Euratom/IST, Lisbon, Portugal.
[2]and University of Toronto, Institute for Aerospace Studies, Canada.

ABSTRACT

The effect of impurity production and recycling on JET hot-ion H-mode discharges is investigated for the MkI and MkII divertors. Analysis of the best of these discharges has been performed with the EDGE2D/NIMBUS codes and the results compared with a wide range of diagnostics. For the very low recycling hot-ion regime, the code predicts that Z_{eff} at the edge (in the upstream SOL) increases with SOL density, and is higher for the MkII than the MkI divertor. These predictions have been confirmed by the experimental data. The significance of the edge density and edge Z_{eff} for the hot-ion regime is that the loss power has been predicted from neoclassical theory to scale as: $P_{Loss} \sim n_{edge}^2 Z_{eff,\ edge}$. It has now been demonstrated that this is consistent with both the MkI and MkII experimental data. It has been observed that the carbon sources in the MkII divertor are increased relative to those in the MkI divertor. These data are compared with the modelled results from the EDGE2D code, taking into account the change in the chemical sputtering yield with the different base temperatures of the MkI (270 °C) and MkII (40 °C) divertors.

1. INTRODUCTION

The hot-ion ELM-free H-mode has achieved the highest fusion performance at JET and has delivered a world record in fusion power during the JET DTE-1 campaign [1]. A systematic reduction in the fusion performance has however been observed between the MkI and MkII divertors. In the present paper a connection is proposed between this observation and the changes in the impurity production between the two divertors. It has been proposed in [2] that the anomalous ion transport within the transport barrier is completely suppressed in the hot-ion H-mode so that the heat flux is controlled by ion neoclassical transport processes. In a recent analysis of long ELM free hot-ion H-modes [3] and steady state ELMy H-modes [4], the width of the transport barrier appears to be proportional to the Larmour radius of the fast ions. Combining this width scaling with the assumption of neoclassical ion losses the following expression for the heat flux through the separatrix (loss power) is obtained: $P_{loss} \approx q_i \approx n_{edge}^2 Z_{eff,edge} I_p^{-1} \sqrt{T_i / E_{fast}}$, where E_{fast} is the average fast particle. Thus, P_{loss} is strongly dependent on the edge density, n_{edge}, and on the Z_{eff} at the edge. It has been observed that the $Z_{eff,edge}$ in MkII is significantly higher than MkI in the hot-ion H-modes.

The low recycling hot ion regime is very different from the high recycling regimes such as ELMy H-mode in 2 respects: 1) $Z_{eff,edge}$ rises with the electron density in the SOL, and 2) screening of impurities produced by physical and chemical sputtering at the divertor targets is very poor, contrary to the high recycling regimes [5]. Modelling with the 2D-fluid EDGE2D code [6] is presented, which confirms these experimental findings. One unexpected result of the MkII operation is that the impurity production yield is about a factor of 2 higher in the MkII divertor than in the MkI divertor. One hypothesis for this elevated sputtering yield is the higher base temperature of the MkII divertor leading to enhanced chemical sputtering. Water cooled rails kept the base temperature of the MkI tiles to 40 °C whereas in MkII thermal isolation from the cooled sub-structure leads to a 270 °C base temperature. Experiments with lower wall temperature in MkII have confirmed this explanation [7].

In this article we report experimental evidence for neoclassical transport inside the edge transport barrier and demonstrate the effect of recycling and impurity behaviour in the hot-ion H-modes. In particular, comparisons of impurity sources in MkI and MkII divertors are presented, as well as detailed modelling using the EDGE2D code and the most recent chemical sputtering data from Mech [8] and Roth [9], taking into account the temperature differences between MkI and MkII divertor targets.

2. EXPERIMENTAL OBSERVATIONS

2.1 Loss power through the separatrix

The power loss through the separatrix is determined by subtracting the radiation inside the separatrix (P_{rad}) and the change in energy content (dW_{dia}/dt) from the neutral beam heating power (P_{NBI}), taking into account the beam shine through loss (P_{sh}), e.g., $P_{loss} = P_{NBI} - dW_{dia}/dt - P_{sh} - P_{rad}$. Fig. 1 plots the loss power, P_{loss}, against the prediction from the neoclassical edge transport barrier model: $P_{loss} \sim n_{edge}^{2} Z_{eff,\ edge}\ Ip^{-1} (T_i/T_{fast})^{1/2}$, for the MkI and MkII hot-ion H-mode discharges. The data are selected from neutral beam (NBI) heated discharges with high fusion performance ($P_{NBI} >$ 15 MW, $W_{dia} \sim$ 10 MJ and D-D reaction rate $R_{DD} > 5{\times}10^{16}\ s^{-1}$). The edge density ($n_{edge}$), is obtained from the edge channel of the interferometer, and $Z_{eff,edge}$ is from the Charge eXchange (CX) diagnostic. There is good agreement with the neoclassical prediction. However, the loss power in MkII, is significantly higher, as a result of the higher $Z_{eff,edge}$ in MkII compared to that in MkI at similar edge densities. It is to be noted that this scaling doesn't take into account the CX losses and losses to the rotation, etc. Detailed TRANSP analysis shows that these extra losses are roughly constant for the high power hot ion H-modes (~5 MW).

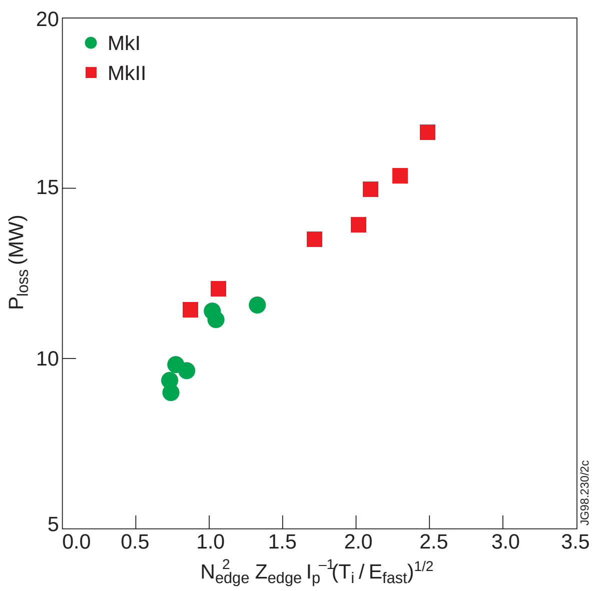

Fig.1 Scaling of loss power, $P_{loss} = P_{in}-P_{sh}-dW/dt-P_{rad}$, for neutral beam heated hot-ion H-mode discharges.

2.2 Comparison of impurity behaviour in MkI and MkII

Fig. 2 compares the average CIII photon flux as a function of the D_α intensity from the outer strike zones for the hot ion H-modes in the MkI and MkII campaigns. The CIII intensity is about a factor of 2 higher in the MkII divertor than that in the MkI divertor for a given D_α flux. The CIII and D_α emissions from the inner divertor show similar results. It is to be noted that the electron temperature at the target plate is very similar for MkI and MkII hot ion discharges with T_e ~ 50 eV at the strike points, as measured by the target Largmuir probes. Therefore, the higher CIII/D_α ratio suggests an increased impurity production yield at the MkII divertor target. As a result, the $Z_{eff,edge}$ is increased significantly with MkII divertor compared to MkI, as illustrated in Fig.3.

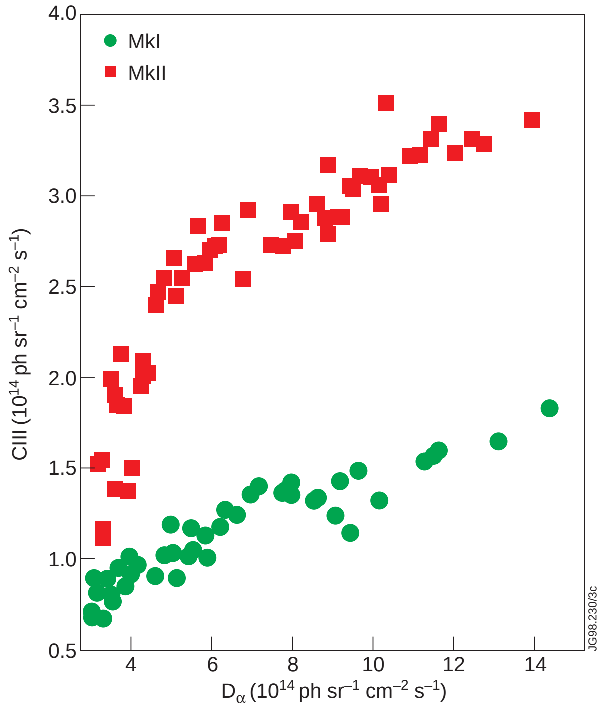

Fig. 2 CIII emissions from outer divertor as a function of the D_α photon fluxes.

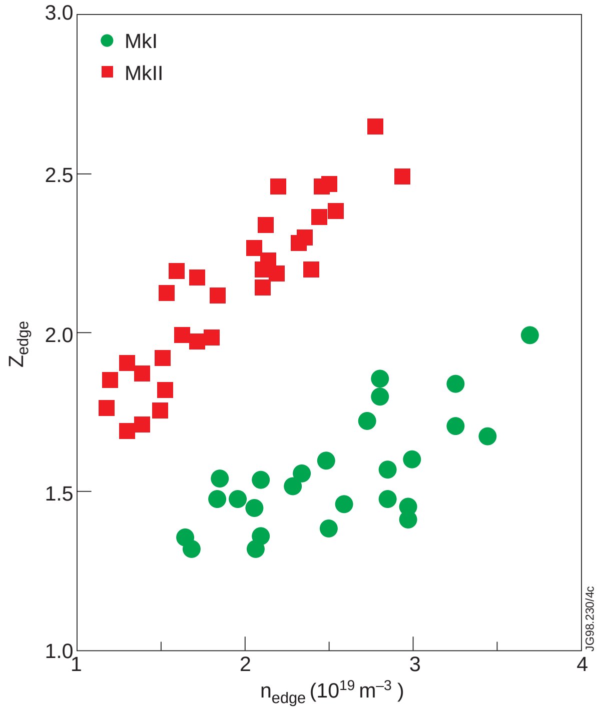

Fig. 3 Comparison of $Z_{eff,edge}$ between MkI and MkII.

2.3 Effect of recycling

One striking feature of the low recycling hot ion regime is that the Z_{eff} at the edge increases as the edge density rises, contrary to the high recycling regimes. This could thus aggravate neo-classical heat loss from the confined plasma core. Fig.4 compares two hot ion H-modes with different recycling levels, two of the best fusion performance discharges in the MkII campaign, #38093 and #38356. These two pulses have similar neutral beam heating power, ~ 18 MW, started from 12s. Pulse 38356 has a higher recycling level compared with pulse 38093, as shown by the vertical D_α signal with the line of sight passing through the outside edge of the plasma. The edge density for pulse 38356 is also higher. After a period of threshold ELMs, Z_{eff} at the edge increases as the edge density rises and is higher for pulse 38356. Indeed, the loss power, P_{loss}, is higher for pulse 38356, compared to the low recycling pulse 38093, as would be expected. Note that in this case P_{loss}, as shown in Fig.4, is determined from the total absorbed power from the neutral beam heating, subtracting dW/dt and the radiation inside the core, taking into account the beam shine through loss, CX losses and loss to rotation, as well as the power stored in the fast ion channel, as obtained from the TRANSP analysis.

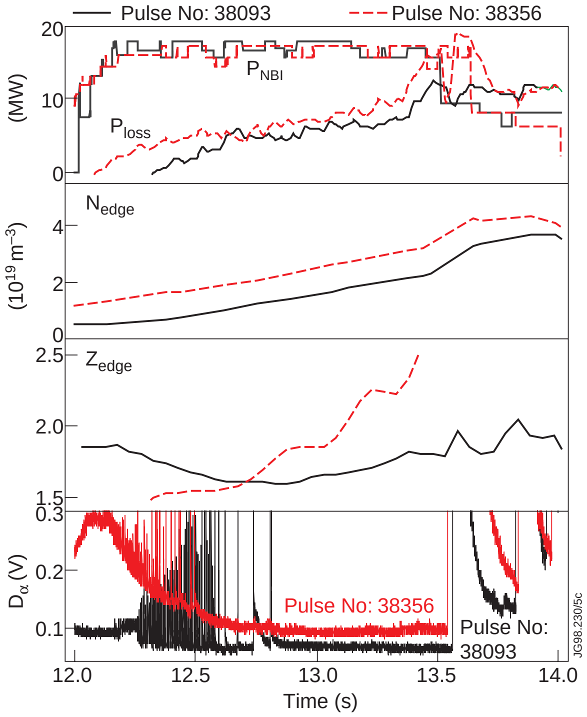

Fig. 4 Time evolution of plasma parameters for pulses 38093 and 38356.

3. EDGE2D MODELLING

In an attempt to understand the effect of the recycling and to assess quantitatively the changes in chemical sputtering yields in MkI and MkII hot-ion H-modes, we have carried out detailed EDGE2D modelling for the discharges described above, # 38093 and # 38356, as well as #33643 which delivered the best fusion performance in MkI. The simulations are performed for the plasmas at the beginning of the ELM-free phase (12.9 s). The outer midplane separatrix density n_{es} and and the power in the ion and electron channels, P_i and P_e, are specified as input to the code. In addition, for cross-field transport, the particle diffusion coefficient is taken to be $D_\perp = 0.1$ m^2/s with an inward pinch velocity, $V_{pinch} = 6.0$ m/s, and $\chi_e = 0.2$ m^2/s, $\chi_i = 0.4$ m^2/s, as used in the previous EDGE2D simulations for the hot-ion H-modes without impurities [10, 11]. Parallel transport is modelled with a 21 moment approach for all species[12]. Toronto'97 chemical sputtering data from Mech et al [6] has been used to compute chemically produced impurities with a given energy of 0.5 eV. However, a yield reduction factor of 0.5 has to be used to match the measured divertor carbon emissions. The average surface temperature for the plasma wetted area is taken to be 400 °C for MkI, which is consistent with the infra red temperature measurements, with a temperature of 300 °C for other areas of the machine. The MkI target temperature rise is also taken to be 100 °C, but with a tile base temperature of 30 °C only.

For the modelling of the low recycling hot ion regime, low n_{es} and P_e are necessary to match the plasma parameters at the target. Fig.5 compares the experimental J_{sat} and T_e profiles at the outer target plate and the modelled results for pulse 38356 with the $n_{es} = 6\times10^{18}$ m^{-3}, and P_i = 5.5 MW, P_e = 0.1 MW as input to the EDGE2D code. The comparison of measured upstream plasma parameters and modelled results are shown in Fig.6. As can be seen, the T_i at upstream

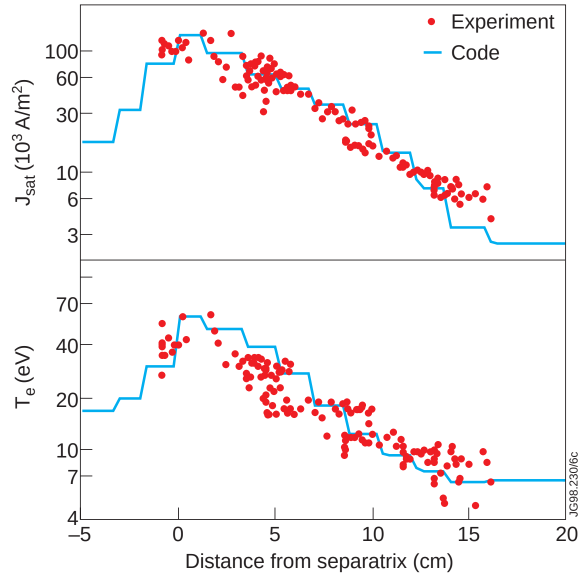

Fig. 5 Comparison of experimental J_{sat} and T_e profiles along the outer target plate and the code predictions for pulse 38356.

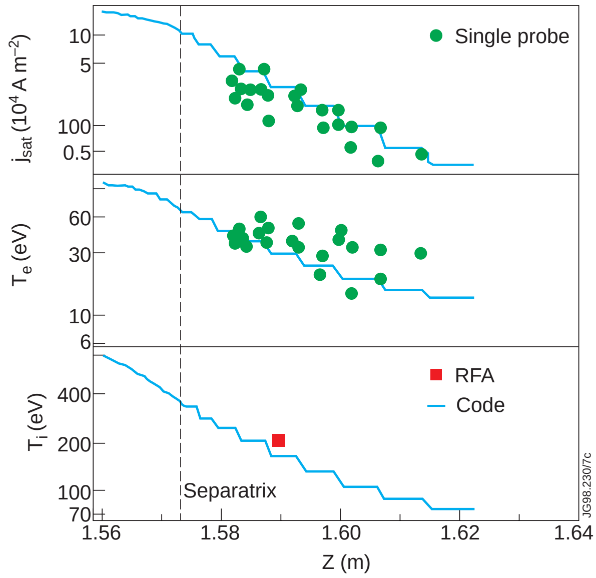

Fig. 6 Comparison of experimental profiles at the upstream and the modelled results for pulse 38356.

(measured by RFA probe) is about a factor of 5 higher than T_e at the upstream and T_e shows little drop along the field line, which is a feature of the sheath-limited regime. Similar levels of agreement are obtained for the lower recycling pulse 38093 with similar values of input power: P_i = 5.0 MW, P_e = 0.1 MW, but with lower separatrix density: $n_{es} = 4.5\times10^{18}$ m^{-3}.

Fig.7 shows the poloidal distribution of the CII photon flux along the divertor target for pulses 38093 and 38356, together with the modelled results. The CII emission in pulse 38356 is significantly higher than pulse 38093. The CIII photon flux, as well as D_α emission, in the divertor are also higher for pulse 38356 and are quantitatively reproduced by the EDGE2D code, as shown in Table I, where the experimental and modelled Z_{eff} at the upstream separatrix are also compared. As can be seen, the higher carbon flux in pulse 38356 results in a higher upstream Z_{eff}. One unexpected feature of this sheath-limited regime is that the $Z_{eff,edge}$ increases with with n_{es}. This is attributed to the increase in the impurity source and poor screening efficiency for divertor impurities, as illustrated in Fig. 8. However, as n_{es} increases sufficiently, the plasma enters the conduction-limited (high recycling) regime, where the shielding for the divertor impurity source is strong enough that the $Z_{eff,edge}$ decreases with n_{es}.

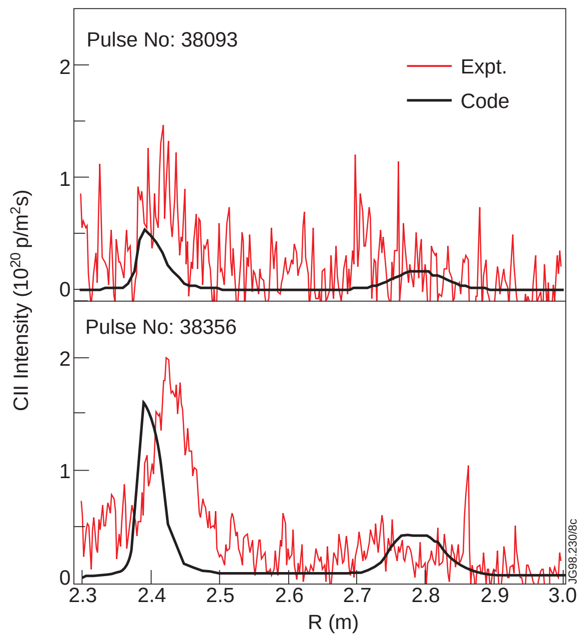

Fig. 7 CII photon fluxes along the divertor target, together with calculated results, for pulses 38093 and 38356.

	38093			38356		
	D_α	CIII (10^{14} p/srm^{2}s)	Z_{edge}	D_α	CIII (10^{14} p/srm^{2}s)	Z_{edge}
expt.	3.6	1.8	1.65	5.9	2.8	1.9
code	3.4	1.6	1.65	5.8	2.9	1.92

Table I Summary of experimental and modelled D_α, CIII intensities from the outer divertor, as well as $Z_{eff,edge}$ at the outer midplane separatrix for #38093 and #38356.

Table II compares divertor sources and $Z_{eff,edge}$ between MkI pulse 38093 and MkII pulse 33643. The loss power for #33643 is similar to #38093, with code input: P_i = 5 MW, P_e = 0.1 MW, n_{es} = 5×10^{18} m^{-3}. The photon yield CIII/D_α in the pulse 38093 (MkII) is about a factor of 2 higher than that in pulse 33643 (MkI). This has been reproduced by the code using the Toronto'97 chemical sputtering data, taking into account the change in the tile temperatures between MkI and MkII divertor targets. In addition, both divertor carbon source and $Z_{eff,edge}$ are also reproduced by the code, as shown in Table II. The newly revised chemical sputtering formula, Roth98 formula [7], can also predict the changes in the chemical sputtering yield between MkI and MkII (Table II). However, the yield predicted by the formula has a much weaker temperature dependence below 600 K, relative to the Toronto'97 data, but increases rapidly from 600 K onwards. It is to be noted that Z_{eff} shows little difference in the high recycling ELMy H-mode discharges in MkI and MkII, where shielding for the divertor impurity source is strong and the wall source dominates [13,14].

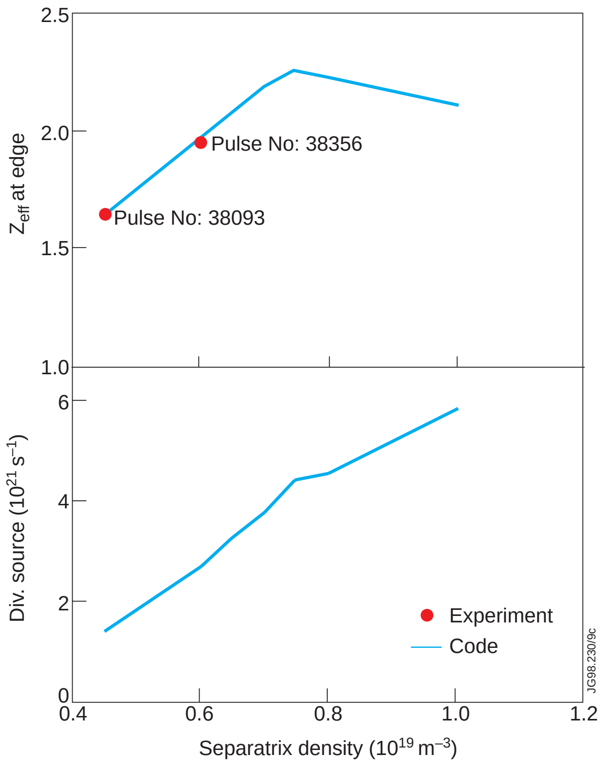

Fig. 8 Divertor carbon source and $Z_{eff,edge}$ as a function of outer midplane separatrix density, calculated with the EDGE2D with P_i=5MW and P_e=0.1MW as input to the code. Experimental data from #38093 and #38356 are also shown.

	33643 (MkI)			38093 (MkII)		
	D_α	CIII (10^{14} p/srm^{2}s)	Z_{edge}	D_α	CIII (10^{14} p/srm^{2}s)	Z_{edge}
expt.	3.0	0.7	1.49	3.6	1.8	1.65
Toronto' 97	2.8	0.8	1.46	3.4	1.6	1.65
Roth' 98	2.6	0.5	1.28	3.3	1.2	1.52

Table II Comparison of experimental D_α, CIII emissions, as well as $Z_{eff,edge}$ together with the code predictions between #33643 (MkI) and #38093 (MkII).

4. CONCLUSIONS

The data from the hot ion H-modes in JET MkI and MkII divertors shows that $P_{Loss} \sim n_{edge}^2 Z_{eff, edge}$, as predicted by the neoclassical theory**.** Z_{eff} at the edge in the hot ion H-mode regime is higher in MkII than that in MkI, leading to the higher loss power in MkII. The carbon fluxes are about a factor of 2 higher in the MkII divertor, at similar divertor plasma electron densities and temperatures, than those in the MkI divertor. This elevated yield is attributed to the enhancement of chemical sputtering at the MkII divertor target, which can be quantitatively reproduced with the EDGE2D code when the higher base temperature of the MkII divertor (270 °C) compared with MkI (40 °C) is taken into account. These higher impurity influxes in the MkII divertor manifest themselves as an increase in the Z_{eff} at the edge due to the inherent poor shielding for the divertor impurities in this particularly low recycling regime. In addition, EDGE2D modelling shows that the upstream separatrix density is correlated with the recycling level. In the low recycling, sheath-limited regime , as the separatrix density rises the predicted $Z_{eff, edge}$ increases, which is consistent with the experimental data from the hot ion H-modes. However, when the edge density is raised sufficiently, the code shows that the plasma enters the high recycling, conduction-limited regime where shielding for impurities is strong and Z_{eff} falls with density, as usually observed.

REFERENCES

[1] P. Lomas et al., to be submitted to Nucl. Fusion (1998).

[2] V. Parail et al., Plasma Phys. and Contr. Fusion 38 (1996) 1421.

[3] H.Y. Guo, V. Parail et al., to be submitted to Nucl. Fusion (1998).

[4] H. Lingertat et al., these Proceedings.

[5] G.F. Matthews et al, *J. Nucl. Mater*. 196-198 (1992) 374.
[6] R. Simonini et al., Contrib. Plasma Phys. 34 (1994)368.
[7] H.Y. Guo, G.F. Matthews, G. Vlases et al., to be submitted to Nucl. Fusion.
[8] B.V. Mech, A.A. Haasz and J.W. Davies, J. Nucl. Mater. 241-243 (1997) 1147.
[9] J. Roth et al., these Proceedings.
[10] A. Taroni et. al., 16th IAEA Fusion Energy Conf., Montréal, Canada, IAEA-CN-64/D3-3 (1996).
[11] G.K. McCormick et al., J. Nucl. Mater. 241-243 (1997) 444.
[12] G. Radford, Contrib. Plasma Phys. 32 (1992) 297.
[13] G.M. McCracken, submitted to Nucl. Fusion (1998).
[14] M. Stamp et al., these Proceedings.